Multichamber Muffler System

Michael Raba, MSc Candidate at University of Kentucky

Created: 2025-09-15 Mon 12:38

Multicomponent Muffler Internal Geometry

Dimensions

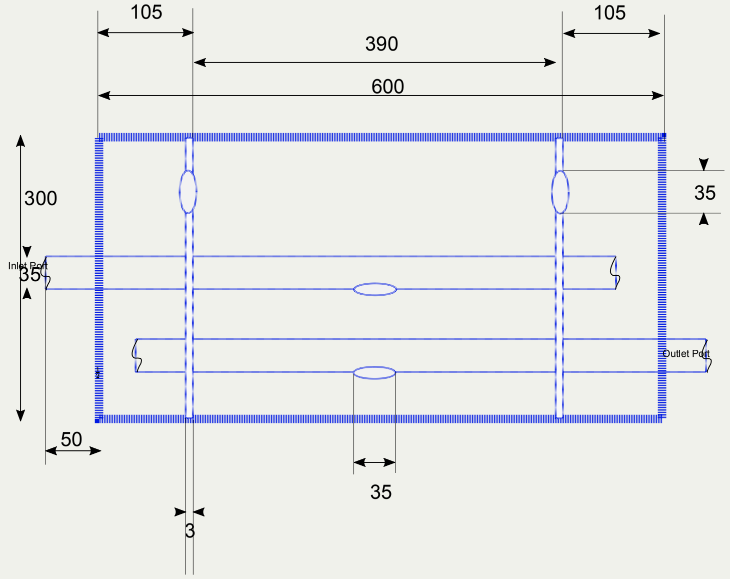

dimensional units in mm

Schematic Variants for Muffler Subcomponents

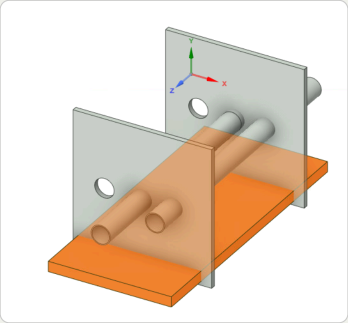

Part 1 — Chamber and Baffle

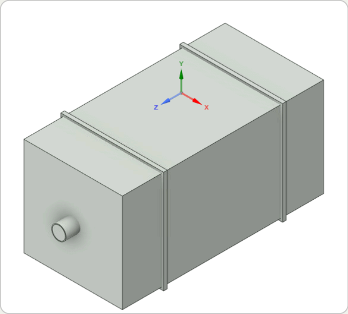

Part 2 — Fluid domain

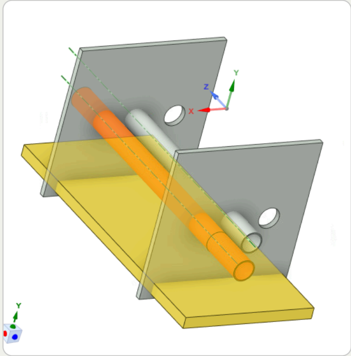

Part 3 — Fiberglass Absorbant (gold)

Part 4 — Showing perforates (aimed at fiberglass)

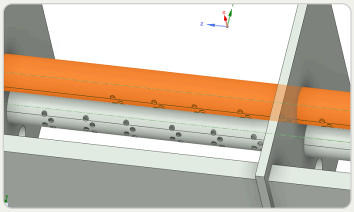

Part 5 — Final Assembly View

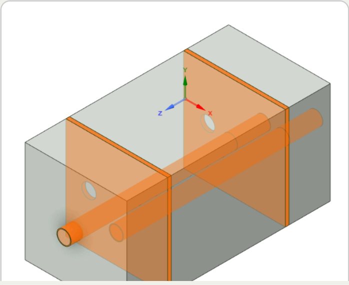

Ansys Simulation

Simulated Transmission Loss (0–1000 Hz) by approximating muffler walls as fluid at 20 deg C

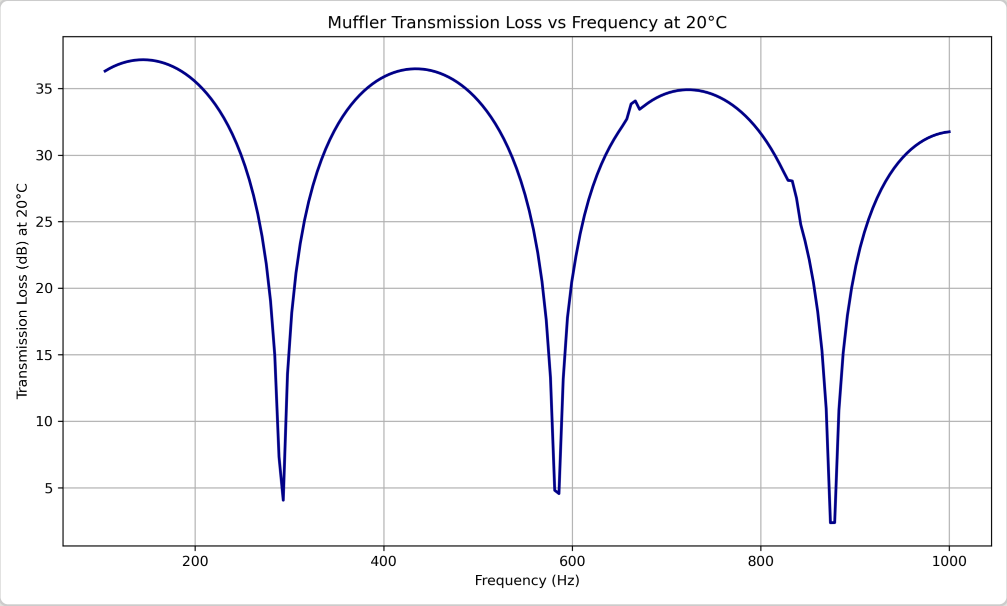

Figure: Transmission Loss curve of the muffler between 5 Hz and 1000 Hz at 20°C.

Simlab Simulation

Simulated Transmission Loss (0–1000 Hz) Simlab model

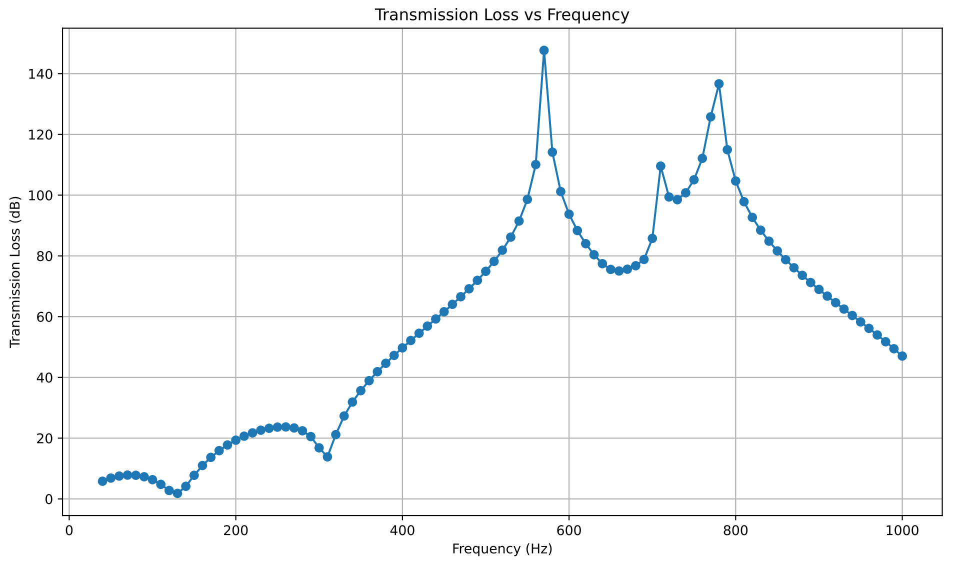

Sidlab and Ansys File Download Center

SIDLAB Model

- **File:** `Mark3Sid.zip`
- **Created with:** SIDLAB 5.1
- **⬇ Download SIDLAB File**

ANSYS Simulation

- **File:** `Mark-I-MDF-clearned-data.wbpz`
- **Created with:** ANSYS 2023 R2
- **⬇ Download ANSYS File**

Sidlab Components

dimensional units in mm

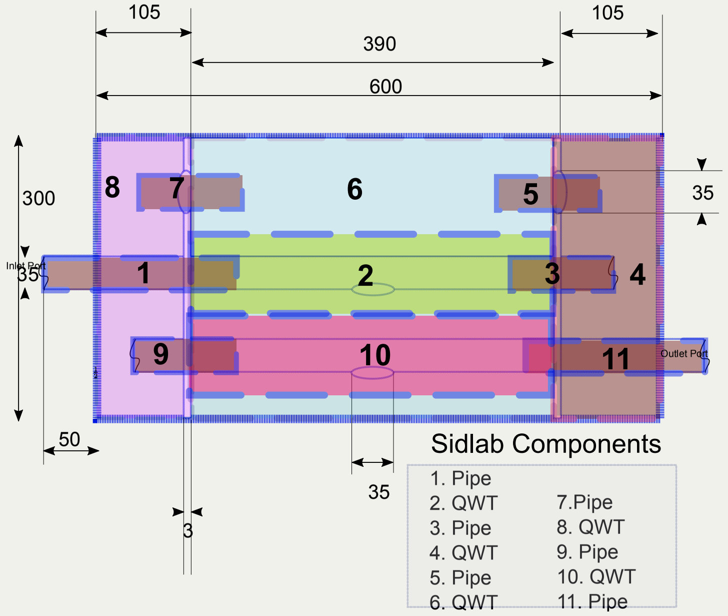

Simulated vs Measured Insertion Loss

Measured vs Simulated TL

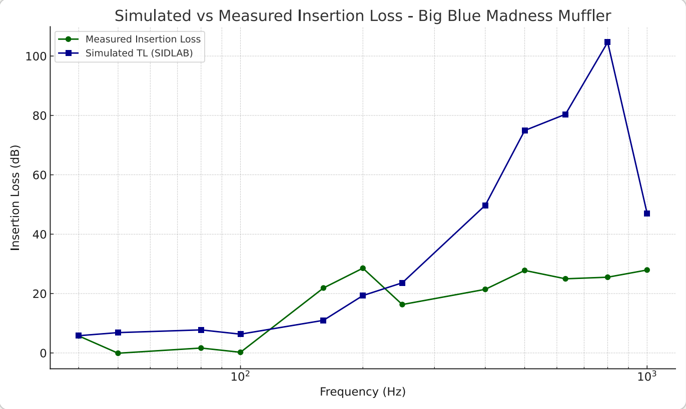

Insertion Loss Explanation

Insertion Loss (IL) quantifies how much sound is attenuated when a muffler is added to the system.

General formula:

$$\mathrm{IL} = 10\log_{10}\left(\frac{P_{\mathrm{baseline}}}{P_{\mathrm{muffler}}}\right)$$

Because our data is already in decibels (dB), this simplifies to:

$$\mathrm{IL} = \mathrm{Power}_{\mathrm{baseline\ (dB)}} - \mathrm{Power}_{\mathrm{muffler\ (dB)}}$$

References

Cited Works

1. Munjal ML. *Acoustics of Ducts and Mufflers*. 2nd ed. Wiley; 2014. ISBN: 9781118443125. https://doi.org/10.1002/9781118443125
2. Dokumacı E. *Duct Acoustics: Fundamentals and Applications to Mufflers and Silencers*. Cambridge University Press; 2021. ISBN: 9781108840750. https://doi.org/10.1017/9781108840750

Note: These references are foundational texts in muffler and duct acoustics and were consulted for system modeling, schematic development, and transmission loss analysis.

Anand Model: Viscoelastoplasticity and its Application to Solder Joints

Michael Raba, MSc Candidate at University of Kentucky

Created: 2025-09-15 Mon 12:39

Source Paper

Constitutive Equations for Hot-Working of Metals

Author: Lallit Anand (1985)

DOI: 10.1016/0749-6419(85)90004-X

One of the foundational papers in thermodynamically consistent viscoplasticity modeling—especially significant in the context of metals subjected to large strains and high temperatures.

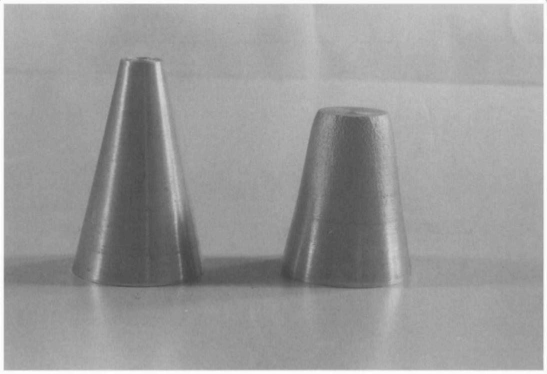

Fig. 25. 1100 aluminum state gradient specimens before and after testing.

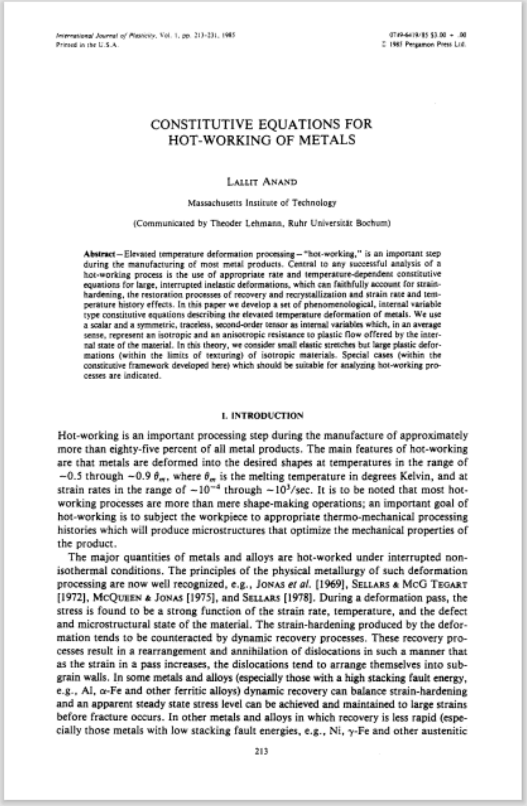

International Journal of Plasticity, Vol. 1, pp. 213-231, 1985
Printed in the U.S.A.

0749-6419/85 $3.00 + .00
© 1985 Pergamon Press Ltd.

CONSTITUTIVE EQUATIONS FOR HOT-WORKING OF METALS

LALLIT ANAND

Massachusetts Institute of Technology

(Communicated by Theoder Lehmann, Ruhr Universität Bochum)

Abstract – Elevated temperature deformation processing – "hot-working," is an important step during the manufacturing of most metal products. Central to any successful analysis of a hot-working process is the use of appropriate rate and temperature-dependent constitutive equations for large, interrupted inelastic deformations, which can faithfully account for strain-hardening, the restoration processes of recovery and recrystallization and strain rate and temperature history effects. In this paper we develop a set of phenomenological, internal variable type constitutive equations describing the elevated temperature deformation of metals. We use a scalar and a symmetric, traceless, second-order tensor as internal variables which, in an average sense, represent an isotropic and an anisotropic resistance to plastic flow offered by the internal state of the material. In this theory, we consider small elastic stretches but large plastic deformations (within the limits of texturing) of isotropic materials. Special cases (within the constitutive framework developed here) which should be suitable for analyzing hot-working processes are indicated.

I. INTRODUCTION

Hot-working is an important processing step during the manufacture of approximately more than eighty-five percent of all metal products. The main features of hot-working are that metals are deformed into the desired shapes at temperatures in the range of ~ 0.5 through $\sim 0.9\,\theta_m$, where θ_m is the melting temperature in degrees Kelvin, and at strain rates in the range of $\sim 10^{-4}$ through $\sim 10^3$/sec. It is to be noted that most hot-working processes are more than mere shape-making operations; an important goal of hot-working is to subject the workpiece to appropriate thermo-mechanical processing histories which will produce microstructures that optimize the mechanical properties of the product.

The major quantities of metals and alloys are hot-worked under interrupted non-isothermal conditions. The principles of the physical metallurgy of such deformation processing are now well recognized, e.g., JONAS *et al.* [1969], SELLARS & MCG TEGART [1972], MCQUEEN & JONAS [1975], and SELLARS [1978]. During a deformation pass, the stress is found to be a strong function of the strain rate, temperature, and the defect and microstructural state of the material. The strain-hardening produced by the deformation tends to be counteracted by dynamic recovery processes. These recovery processes result in a rearrangement and annihilation of dislocations in such a manner that as the strain in a pass increases, the dislocations tend to arrange themselves into sub-grain walls. In some metals and alloys (especially those with a high stacking fault energy, e.g., Al, α-Fe and other ferritic alloys) dynamic recovery can balance strain-hardening and an apparent steady state stress level can be achieved and maintained to large strains before fracture occurs. In other metals and alloys in which recovery is less rapid (especially those metals with low stacking fault energies, e.g., Ni, γ-Fe and other austenitic

Case Study: Wang (2001) Apply to Solder

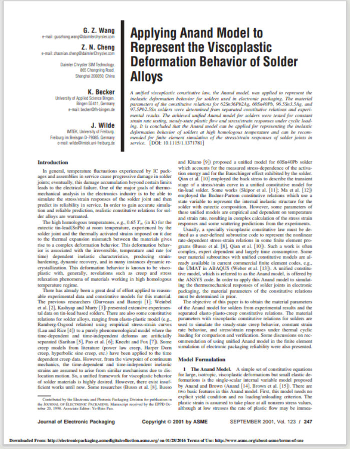

G. Z. Wang
e-mail: guozhong.wang@daimlerchyrsler.com

Z. N. Cheng
e-mail: zhaonian.cheng@daimlerChrysler.com

Daimler Chrysler SIM Technology,
865 Changning Road,
Shanghai 200050, China

K. Becker
University of Applied Science Bingen,
Bingen 55411, Germany
e-mail: becker@fh-bingen.de

J. Wilde
IMTEK, University of Freiburg,
Freiburg im Breisgan D-79085, Germany
e-mail: wilde@imtek.uni-freiburg.de

Applying Anand Model to Represent the Viscoplastic Deformation Behavior of Solder Alloys

A unified viscoplastic constitutive law, the Anand model, was applied to represent the inelastic deformation behavior for solders used in electronic packaging. The material parameters of the constitutive relations for 62Sn36Pb2Ag, 60Sn40Pb, 96.5Sn3.5Ag, and 97.5Pb2.5Sn solders were determined from separated constitutive relations and experimental results. The achieved unified Anand model for solders were tested for constant strain rate testing, steady-state plastic flow and stress/strain responses under cyclic loading. It is concluded that the Anand model can be applied for representing the inelastic deformation behavior of solders at high homologous temperature and can be recommended for finite element simulation of the stress/strain responses of solder joints in service. [DOI: 10.1115/1.1371781]

Introduction

In general, temperature fluctuations experienced by IC packages and assemblies in service cause progressive damage in solder joints; eventually, this damage accumulation beyond certain limits leads to the electrical failure. One of the major goals of thermomechanical analysis in the electronics industry is to be able to simulate the stress/strain responses of the solder joint and then predict its reliability in service. In order to gain accurate simulation and reliable prediction, realistic constitutive relations for solder alloys are warranted.

The high homologous temperatures, e.g., 0.65 T_m (in K) for the eutectic tin-lead(SnPb) at room temperature, experienced by the solder joint and the thermally activated strains imposed on it due to the thermal expansion mismatch between the materials gives rise to a complex deformation behavior. This deformation behavior is associated with the irreversible, temperature and rate (or time) dependent inelastic characteristics, producing strain-hardening, dynamic recovery, and in many instances dynamic recrystallization. This deformation behavior is known to be viscoplastic with, generally, revelations such as creep and stress relaxation phenomena of materials working in high homologous temperature regime.

There has already been a great deal of effort applied to reasonable experimental data and constitutive models for this material. The previous researchers (Darveaux and Banerji [1]; Weinbel et al. [2], Kashyap and Murty [3]) presented extensive experimental data on tin-lead based solders. There are also some constitutive relations for solder alloys, ranging from elasto-plastic model (e.g., Ramberg-Osgood relation) using empirical stress-strain curves (Lau and Rice [4]) to a purely phenomenological model where the time-dependent and time-independent deforms are artificially separated (Sarihan [5], Pao et al. [6]; Knecht and Fox [7]). Some creep models from literature (power law creep, Harper Dorn creep, hyperbolic sine creep, etc.) have been applied to the time dependent creep data. However, from the viewpoint of continuum mechanics, the time-dependent and time-independent inelastic strains are assumed to arise from similar mechanisms due to dislocation motion. So, a unified framework for viscoplastic behavior of solder materials is highly desired. However, there exist insufficient works until now. Some researches (Busso et al. [8], Busso and Kitano [9]) proposed a unified model for 60Sn40Pb solder which accounts for the measured stress-dependence of the activation energy and for the Bauschinger effect exhibited by the solder. Qian et al. [10] employed the back stress to describe the transient stage of a stress/strain curve in a unified constitutive model for tin-lead solder. Some works (Skipor et al. [11]; Ma et al. [12]) employed the Bodner-Partom constitutive relations which use a state variable to represent the internal inelastic structure for the solder with eutectic composition. However, some parameters of these unified models are empirical and dependent on temperature and strain rate, resulting in complex calculation of the stress strain responses and some scattering predictions from the experiments.

Usually, a specially viscoplastic constitutive law must be defined as a user-defined subroutine code to represent the nonlinear rate-dependent stress-strain relations in some finite element programs (Busso et al. [8], Qian et al. [10]). Such a work is often complex, expert dependent and largely time consumptive. Some user material subroutines with unified constitutive models are already available in current commercial finite element codes, e.g., the UMAT in ABAQUS (Weber et al. [13]). A unified constitutive model, which is referred to as the Anand model, is offered by the ANSYS code. In order to apply this Anand model to simulating the thermomechanical responses of solder joints in electronic packaging, the material parameters of the constitutive relations must be determined in prior.

The objective of this paper is to obtain the material parameters of the Anand model for solders from experimental results and the separated elasto-plasto-creep constitutive relations. The material parameters with viscoplastic constitutive relations for solders are used to simulate the steady-state creep behavior, constant strain rate behavior, and stress/strain responses under thermal cyclic loading for comparison and verification. Some discussions on recommendation of using unified Anand model in the finite element simulation of electronic packaging reliability were also presented.

Model Formulation

1 The Anand Model. A simple set of constitutive equations for large, isotropic, viscoplastic deformations but small elastic deformations is the single-scalar internal variable model proposed by Anand and Brown (Anand [14], Brown et al. [15]). There are two basic features in this Anand model. First, this model needs no explicit yield condition and no loading/unloading criterion. The plastic strain is assumed to take place at all nonzero stress values, although at low stresses the rate of plastic flow may be immea-

Contributed by the Electronic and Photonic Packaging Division for publication in the JOURNAL OF ELECTRONIC PACKAGING. Manuscript received by the EPPD October 20, 1998. Associate Editor: Ye-Hein Pao.

Journal of Electronic Packaging SEPTEMBER 2001, Vol. 123 / **247**

Source: Wang, C. H. (2001). “A Unified Creep–Plasticity Model for Solder Alloys.”
DOI: 10.1115/1.1371781

Why Wang's Paper Matters

- Applies Anand’s unified viscoplastic framework to model solder behavior.
- Anand's model can be reduced and fitted from experiments.
- transition the theory into engineering-scale implementation.
- Targets solder joints in microelectronic packages (chip on PCB, soldered connections).

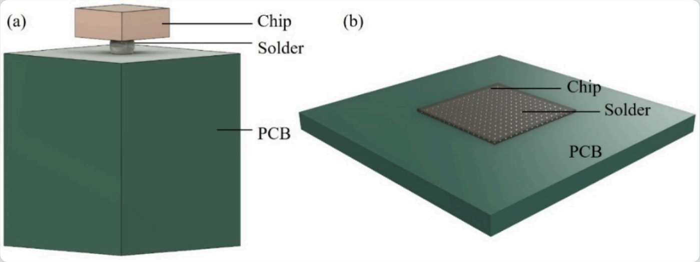

Comparing Anand Model Predictions at Two Strain Rates

Observed Behavior

- **Top Graph (a):** $\dot{\varepsilon} = 10^{-2}\,\mathrm{s}^{-1}$
- High strain rate → higher stress
- Recovery negligible → pronounced hardening
- **Bottom Graph (b):** $\dot{\varepsilon} = 10^{-4}\,\mathrm{s}^{-1}$
- Lower strain rate → lower stress at same strain
- Recovery and creep effects more significant

Model Accuracy: Lines = model prediction, X = experimental data

Key Insights from Wang (2001)

- “At lower strain rates, recovery dominates… the stress levels off early.”
- “At high strain rates, hardening dominates, and the stress grows continuously.”

Anand’s model smoothly captures strain-rate and temperature dependence of solder materials.

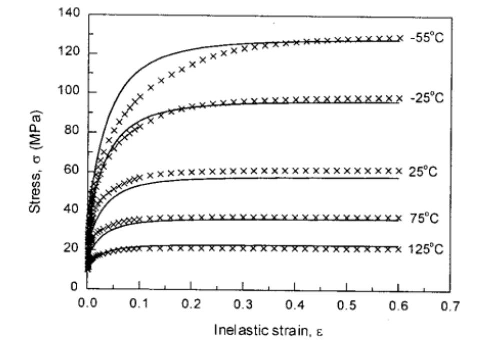

(a) $\dot{\varepsilon}=1.0\times10^{-2}\ \mathrm{s}^{-1}$

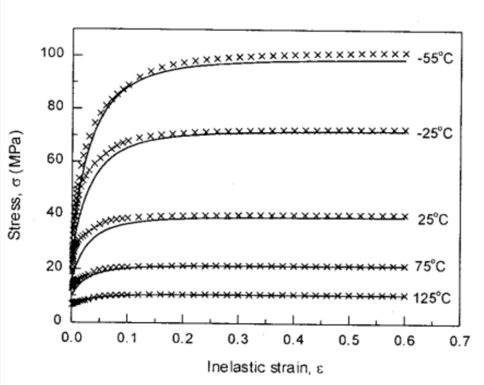

(b) $\dot{\varepsilon}=1.0\times10^{-4}\ \mathrm{s}^{-1}$

Main Equations of Wang's Anand-Type Viscoplastic Model

Flow Rule (Plastic Strain Rate)

- $$\dot{\varepsilon}^p = A \exp\left(-\frac{Q}{RT}\right)\left[\sinh\left(\frac{j\sigma}{s}\right)\right]^{1/m}$$
- Plastic strain rate increases with stress and temperature.
- No explicit yield surface; flow occurs at all nonzero stresses.

Deformation Resistance Saturation s^*

- $$s^* = \hat{s}\left(\frac{\dot{\varepsilon}^p}{A}\exp\left(\frac{Q}{RT}\right)\right)^n$$
- Defines the steady-state value that s evolves toward.
- Depends on strain rate and temperature.

Evolution of Deformation Resistance s

- $$\dot{s} = h_0\left|1 - \frac{s}{s^*}\right|^a \operatorname{sign}\left(1 - \frac{s}{s^*}\right)\dot{\varepsilon}^p$$
- Describes dynamic hardening and softening of the material.
- s evolves depending on proximity to s^* and flow activity.

Note: Constants $A, Q, m, j, h_0, \hat{s}, n, a$ are material-specific and fitted to experimental creep/strain rate data.

Anand Viscoplasticity Constants for 60Sn40Pb

Image Reference

Values are from correspond to 60Sn40Pb solder parameters used in Anand's model:

- S_0: Initial deformation resistance
- Q/R: Activation energy over gas constant
- A: Pre-exponential factor for flow rate
- ξ: Multiplier of stress inside sinh
- m: Strain rate sensitivity of stress
- h_0: Hardening/softening constant
- $\hat{s}$: Coefficient for saturation stress
- n: Strain rate sensitivity of saturation
- a: Strain rate sensitivity of hardening or softening

Numerical Values

- $S_0 = 5.633 \times 10^7$ Pa
- $Q/R = 10830$ K
- $A = 1.49 \times 10^7$ s^{-1}
- $\xi = 11$
- $m = 0.303$
- $h_0 = 2.6408 \times 10^9$ Pa
- $\hat{s} = 8.042 \times 10^7$ Pa
- $n = 0.0231$
- $a = 1.34$

These constants match Wang's paper for modeling 60Sn40Pb viscoplasticity.

Forward Euler Explicit time integration scheme Pseudocode

Initialization

- Material constants: $A, Q/R, j, m, h_0, \hat{s}, n, a, E$
- Strain rate: $\dot{\varepsilon}$
- Temperature set: $\{T_i\}$
- Set: $\varepsilon^p(0) = 0, \quad s(0) = \hat{s}$

Time Evolution Loop

```
1. $\varepsilon_{\text{total}}(t) = \dot{\varepsilon}\, t$
2. $\sigma_{\text{trial}} = E(\varepsilon_{\text{total}} - \varepsilon^p)$
3. Compute $x = \frac{j\sigma}{s}$
4. Approximate $\sinh(x)$ (linearize if $|x| \ll 1$)
5. $\dot{\varepsilon}^p = Ae^{-Q/RT}(\sinh(x))^{1/m}$
```

Plastic Flow & Resistance Evolution

```
6. $s^* = \hat{s}\left(\frac{\dot{\varepsilon}^p}{A} e^{Q/RT}\right)^n$
7. $\dot{s} = h_0 \left|1 - \frac{s}{s^*}\right|^a \operatorname{sign}\left(1 - \frac{s}{s^*}\right) \dot{\varepsilon}^p$
8. Update: $\varepsilon^p(t + \Delta t) = \varepsilon^p(t) + \dot{\varepsilon}^p \Delta t$
9. Update: $s(t + \Delta t) = s(t) + \dot{s}\, \Delta t$
10. Record $(\varepsilon_{\text{total}}, \sigma_{\text{trial}})$
```

Termination

- Stop when $\varepsilon_{\text{total}} \geq \varepsilon_{\max}$
- Plot σ vs ε for all T_i

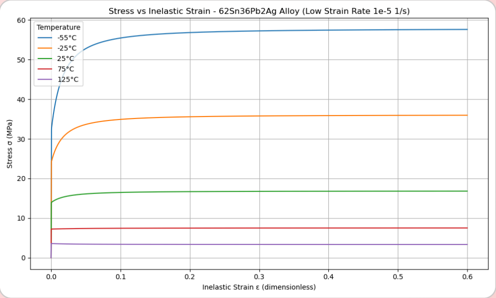

Forward Euler Scheme for Anand Model

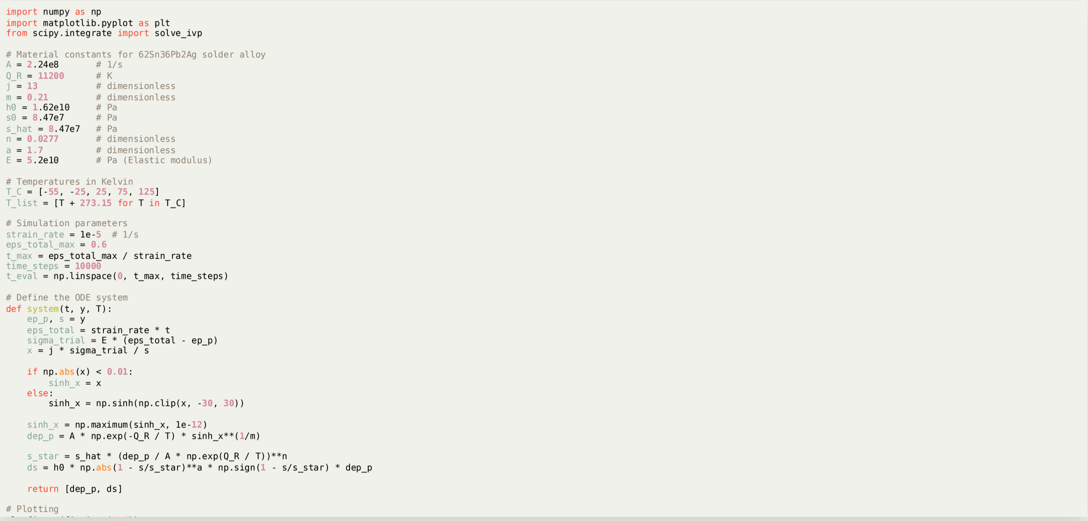

```python
import numpy as np
import matplotlib.pyplot as plt
from scipy.integrate import solve_ivp

# Material constants for 62Sn36Pb2Ag solder alloy
A = 2.24e8       # 1/s
Q_R = 11200      # K
j = 13           # dimensionless
m = 0.21         # dimensionless
h0 = 1.62e10     # Pa
s0 = 8.47e7      # Pa
s_hat = 8.47e7   # Pa
n = 0.0277       # dimensionless
a = 1.7          # dimensionless
E = 5.2e10       # Pa (Elastic modulus)

# Temperatures in Kelvin
T_C = [-55, -25, 25, 75, 125]
T_list = [T + 273.15 for T in T_C]

# Simulation parameters
strain_rate = 1e-5  # 1/s
eps_total_max = 0.6
t_max = eps_total_max / strain_rate
time_steps = 10000
t_eval = np.linspace(0, t_max, time_steps)

# Define the ODE system
def system(t, y, T):
    ep_p, s = y
    eps_total = strain_rate * t
    sigma_trial = E * (eps_total - ep_p)
    x = j * sigma_trial / s

    if np.abs(x) < 0.01:
        sinh_x = x
    else:
        sinh_x = np.sinh(np.clip(x, -30, 30))

    sinh_x = np.maximum(sinh_x, 1e-12)
    dep_p = A * np.exp(-Q_R / T) * sinh_x**(1/m)

    s_star = s_hat * (dep_p / A * np.exp(Q_R / T))**n
    ds = h0 * np.abs(1 - s/s_star)**a * np.sign(1 - s/s_star) * dep_p

    return [dep_p, ds]

# Plotting
```

Strain rate sensitivity of stress m

- As $m \to 0$, rate insensitive (yield)
- As $m \to 1$, small stress change causes big change in strain rate

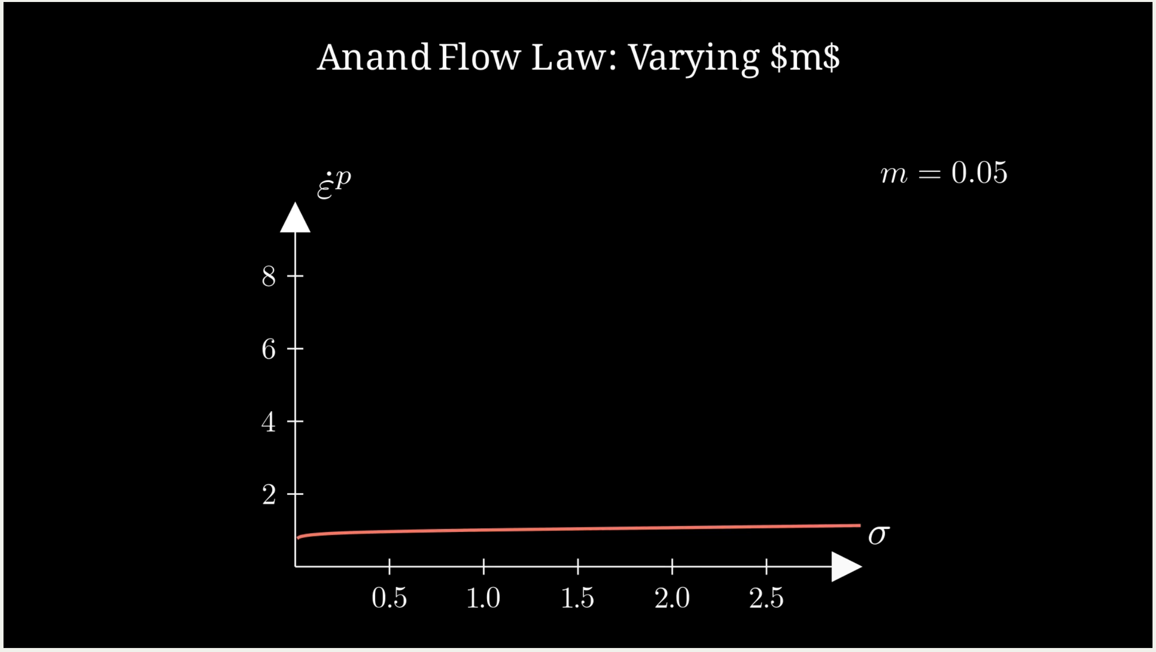

Flow rule

Tensorial Flow Rule (directional form)

$$\mathbf{D}^p = \dot{\epsilon}^p \left(\frac{3}{2} \frac{\mathbf{T}'}{\bar{\sigma}} \right)$$

Equivalent Stress Definition

$$\bar{\sigma} = \sqrt{\frac{3}{2} \mathbf{T}' : \mathbf{T}'}$$

Plastic Strain Rate (magnitude form)

$$\dot{\epsilon}^p = A \exp\left(-\frac{Q}{R\theta} \right) \left[\sinh\left(\xi \frac{\bar{\sigma}}{s} \right) \right]^{1/m}$$

Full Flow Rule with Hyperbolic Sine

$$\mathbf{D}^p = A \exp\left(-\frac{Q}{R\theta} \right) \left[\sinh\left(\xi \frac{\bar{\sigma}}{s} \right) \right]^{1/m} \left(\frac{3}{2} \frac{\mathbf{T}'}{\bar{\sigma}} \right),$$

$$= \dot{\gamma}^p \left(\frac{\widetilde{\mathbf{T}}'}{2\bar{\tau}} \right), \quad \bar{\tau} = \left\{ \frac{1}{2} \mathrm{tr}(\widetilde{\mathbf{T}}'^2) \right\}^{1/2}$$

Summary:

- Direction given by $\mathbf{T}'$.
- Magnitude determined by hyperbolic sine based on $\bar{\sigma}/s$.
- $\bar{\tau}$ represents the effective shear stress computed from deviatoric stress.
- $\bar{\sigma} = \sqrt{\frac{3}{2}\mathbf{T}' : \mathbf{T}'}$ is the von Mises Equivalent stress, but is formally defined without yield point
- Full flow = **direction × magnitude**.

Evolution Equation for the Stress

Stress Evolution Equation (Rate form of Hooke's Law)

$$\overset{\nabla}{\mathbf{T}} = \mathbb{L}\left[\mathbf{D} - \mathbf{D}^p\right] - \mathbf{\Pi}\dot{\theta}$$

(rate-form Hooke’s law for finite deformation plasticity, with frame-indifference enforced through the Jaumann rate.)

Jaumann Rate Definition

$$\overset{\nabla}{\mathbf{T}} = \dot{\mathbf{T}} - \mathbf{W}\mathbf{T} + \mathbf{T}\mathbf{W}$$

Material Tensors and Operators

- $\mathbb{L} = 2\mu\mathbf{I} + \left(\kappa - \frac{2}{3}\mu\right) \mathbf{1} \otimes \mathbf{1}$ — isotropic elasticity tensor
- $\mathbb{L}\mathbf{D}$ represents how instantaneous strain rates generate stresses according to the elastic material's stiffness properties.
- $\mu = \mu(\theta)$, $\kappa = \kappa(\theta)$ — temperature-dependent moduli
- $\mathbf{\Pi} = (3\alpha\kappa)\mathbf{1}$ — stress-temperature coupling
- $\alpha = \alpha(\theta)$ — thermal expansion coefficient
- $\mathbf{D} = \mathrm{sym}(\nabla\mathbf{v})$ — stretching tensor
- $\mathbf{W} = \mathrm{skew}(\nabla\mathbf{v})$ — spin tensor
- $\mathbf{I}$ = fourth-order identity tensor
- $\mathbf{1}$ = second-order identity tensor

Summary:

- Stress rate follows Jaumann derivative to ensure frame indifference.
- Elastic response governed by isotropic fourth-order tensor $\mathbb{L}$.
- Thermal expansion introduces additional stress through $\mathbf{\Pi}\dot{\theta}$.

Stress Evolution and Thermal Effects

Stress Evolution and Thermal Effects

In the stress evolution equation,

$$\overset{\nabla}{\mathbf{T}} = \mathbb{L}\left[\mathbf{D} - \mathbf{D}^p\right] - \mathbf{\Pi}\dot{\theta},$$

the term $\mathbf{\Pi}\dot{\theta}$ represents the stress change that would occur due to pure thermal expansion alone, without any mechanical loading.

Why Subtract the Thermal Term?

- Thermal expansion creates strain even without external forces.
- Without subtracting $\mathbf{\Pi}\dot{\theta}$, the model would falsely attribute thermal strain as mechanical stress.
- Subtracting isolates the true mechanical response from thermal effects.

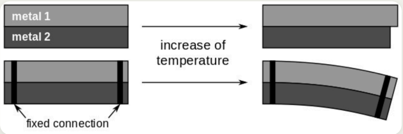

Summary:

- Thermal expansion induces strain without force.
- Subtracting $\mathbf{\Pi}\dot{\theta}$ ensures only mechanical strains generate stresses.
- This keeps the constitutive model physically accurate during heating and cooling.

Relaxed (Intermediate) Configuration

Context for the Relaxed Configuration

- The relaxed configuration represents the material after removing plastic deformations but before applying new elastic deformations.
- It is introduced to separate permanent plastic effects from recoverable elastic effects.
- All thermodynamic potentials, internal variables, and evolution laws are defined relative to this frame.
- The relaxed state provides a clean, natural reference for measuring elastic strain E^e and computing dissipation.

What Happens in the Relaxed Configuration?

- The elastic deformation gradient F^e is measured from the relaxed state to the current deformed state.
- Elastic strain measures like C^e and E^e are defined in this configuration.
- The Kirchhoff stress $\widetilde{\mathbf{T}}$ is naturally associated with the relaxed volume.
- Plastic flow is accounted for separately through the plastic velocity gradient $\mathbf{L}^p$.

Summary:

- The relaxed configuration isolates elastic responses cleanly, enabling proper definition of thermodynamics and plastic evolution laws.

Relaxed Configuration Constituative Laws

Kinematics in the Relaxed Configuration

- Elastic deformation gradient:

$$F = F^e F^p \quad \Rightarrow \quad F^e = F F^{p-1}$$

- Elastic right Cauchy-Green tensor:

$$C^e = F^{eT} F^e$$

- Elastic Green–Lagrange strain tensor:

$$E^e = \frac{1}{2}(C^e - I)$$

Stress and Power Quantities

- Kirchhoff stress (weighted Cauchy stress):

$$\widetilde{\mathbf{T}} = (\det F)\mathbf{T}$$

- Stress power split:

$$\dot{\omega} = \dot{\omega}^e + \dot{\omega}^p$$

$$\dot{\omega}^e = \widetilde{\mathbf{T}} : \dot{E}^e \quad , \quad \dot{\omega}^p = (C^e \widetilde{\mathbf{T}}) : \mathbf{L}^p$$

Summary:

- Elastic kinematics and stress measures are formulated relative to the relaxed configuration, cleanly separating plastic and elastic contributions.
- Stress Power Split allows Anand to cleanly isolate plastic dissipation from elastic storage.
- Green-Lagrange strain tensor E^e is used because it symmetrically captures nonlinear elastic strain relative to the relaxed configuration
- The right Cauchy-Green tensor $C^e = F^{e^T} F^e$ is required as an intermediate to compute E^e from the elastic deformation gradient F^e without referencing spatial coordinates

Dissipation Separation: Elastic vs Plastic in Anand's Model

Thermodynamic Separation

1. **Start with Total Dissipation:**

$$\mathcal{D} = \dot{\omega} - \dot{\psi} \geq 0$$

where $\dot{\omega} = \widehat{\mathbf{T}} : \dot{\mathbf{E}}^e + (\mathbf{C}^e \widehat{\mathbf{T}}) : \mathbf{L}^p$

2. **Split Stress Power:**

$$\dot{\omega} = \dot{\omega}^e + \dot{\omega}^p$$

with:

- $\dot{\omega}^e = \widehat{\mathbf{T}} : \dot{\mathbf{E}}^e$
- $\dot{\omega}^p = (\mathbf{C}^e \widehat{\mathbf{T}}) : \mathbf{L}^p$

3. **Group Terms with $\dot{\psi}$:**

$$(\dot{\omega}^e - \dot{\psi}) + \dot{\omega}^p \geq 0$$

4. **Apply Elastic Energy Consistency:**

$$\dot{\omega}^e - \dot{\psi} = 0 \quad \Rightarrow \quad \dot{\omega}^p \geq 0$$

Key Physical Insights

- **Elastic deformations** are recoverable and do not cause entropy production.
- **All dissipation** stems from the plastic flow: $\dot{\omega}^p$.
- **Plastic work** increases entropy and governs viscoplastic evolution.

Summary:
The stress power split ensures that the second law is satisfied by assigning dissipation solely to irreversible processes.

Reference Configuration

Framework in the Reference Configuration

- The free energy ψ is defined relative to the reference configuration.
- State variables like $E^e, \theta, \bar{g}, \bar{\mathbf{B}}, s$ are used as arguments of ψ.
- Stress is expressed using the second Piola–Kirchhoff tensor $\mathbf{S}$.
- Dissipation inequality, stress–strain relations, and evolution laws are all written in reference variables.
- Mass density ρ_0 from the reference configuration normalizes all terms.

Key Equations in the Reference Frame

- Free energy:

$$\boxed{\psi = \psi(E^e, \theta, \bar{g}, \bar{\mathbf{B}}, s)}$$

- Dissipation inequality:

$$\boxed{\dot{\psi} + \eta\dot{\theta} - \rho_0^{-1}\mathbf{S} : \dot{E} + (\rho_0\theta)^{-1}\mathbf{q}_0 \cdot \mathbf{g}_0 \leq 0}$$

- Constitutive relation:

$$\boxed{\mathbf{S} = \rho_0 \frac{\partial \psi}{\partial E^e}}$$

Summary:

- In the reference configuration, all energy storage, stress updates, and internal variable evolution are formulated with reference-frame quantities for consistency and objectivity.

Thermodynamic Quantities

- Free energy density:

$$\boxed{\psi = \epsilon - \theta\eta}$$

- Reduced dissipation inequality:

$$\boxed{\dot{\psi} + \eta\dot{\theta} - \rho^{-1}\mathbf{T} : \mathbf{L} + (\rho\theta)^{-1}\mathbf{q} \cdot \mathbf{g} \leq 0}$$

- State variables:

$$\{E^{e}, \theta, \bar{g}, \bar{\mathbf{B}}, s\}$$

with E^{e} as elastic strain and s as internal resistance.

Stress Power and Kirchhoff Stress

- Stress power per relaxed volume:

$$\boxed{\dot{\omega} = \left(\frac{\rho_0}{\rho}\right)\mathbf{T} : \mathbf{L}}$$

- Weighted Cauchy (Kirchhoff) stress:

$$\boxed{\widetilde{\mathbf{T}} = (\det F)\mathbf{T}} \quad \text{or} \quad \boxed{\widetilde{\mathbf{T}} = \left(\frac{\rho_0}{\rho}\right)\mathbf{T}}$$

- Decomposition of stress power:

$$\boxed{\dot{\omega} = \dot{\omega}^{e} + \dot{\omega}^{p}}$$

$$\dot{\omega}^{e} = \widetilde{\mathbf{T}} : \dot{E}^{e}, \quad \dot{\omega}^{p} = (C^{e}\widetilde{\mathbf{T}}) : \mathbf{L}^{p}$$

Summary:
- Free energy and dissipation govern thermodynamic consistency.
- Stress power naturally splits into elastic and plastic parts.
- Kirchhoff stress simplifies stress evolution accounting for volume changes.

POD Analysis of Turbulent Pipe Flow

M. Raba

Created: 2025-09-15 Mon 12:39

1. Code Execution and Layout

1.1. Layout

1. b7.m
2. initSpectral.m
    - reads in binary files, takes eg m-fft
3. ↪ initEigs.m
    - forms corrMat, finds eigenvalues

1.2. Layout 2

1. ↪ initPod.m
    - carries out POD calculations (quadrature, multiplication ggf betwen $\alpha\Phi$) according to Papers (Citriniti George 2000 for Classic POD, Hellstrom Smits 2017 for Snapshot POD)
2. ↪ timeReconstructFlow.m
    - performs 2d reconstruction + plotSkmr (generates 1d radial graph)

1.3. Important Switches

pipe = Pipe(); creates a Pipe Class. As the functions (above) are called, data is stored in sub-structs:

1. obj.CaseId - stores properties like Re, rotation number S, experimental flags such as quadrature (simpson/trapezoidal), number of gridpoints, frequently called vectors (rMat $r = 1, \dots, 0.5$)
2. obj.pod - eigen data, used for calculating POD
3. obj.solution - computed POD modes
4. obj.plt - plot configuration

2. Equations Used in Code Procedure

2.1. Classic POD Equations

The following equations are used in the above code.

$$\int_{r'} \mathbf{S}\left(k;m;r,r'\right)\Phi^{(n)}\left(k;m;r'\right)r'\mathrm{d}r' = \lambda^{(n)}(k;m)\Phi^{(n)}(k;m;r)$$

$$\mathbf{S}\left(k;m;r,r'\right) = \lim_{\tau\to\infty}\frac{1}{\tau}\int_0^{\tau}\mathbf{u}(k;m;r,t)\mathbf{u}^*\left(k;m;r',t\right)\mathrm{d}t$$

$$\alpha^{(n)}(k;m;t) = \int_r \mathbf{u}(k;m;r,t)\Phi^{(n)^*}(k;m;r)r\,\mathrm{d}r$$

2.2. Classic POD Equations (Fixed)

$$\int_{r'} \underbrace{r^{1/2} S_{i,j}\left(r, r'; m; f\right) r'^{1/2}}_{W_{i,j}(r,r';m;f)} \underbrace{\phi_j^{*(n)}\left(r'; m; f\right) r'^{1/2}}_{\hat{\phi}_j^{\psi(i)}(r';m;f)} \mathrm{d}r'$$

$$= \underbrace{\lambda^{(n)}(m, f)}_{\hat{\lambda}^{(n)}(m;f)} \underbrace{r^{1/2} \phi_i^{(n)}(r; m; f)}_{\hat{\phi}_i^{(n)}(r,m;f)}$$

$$\alpha_n(m;t) = \int_r \mathbf{u}(m;r,t) r^{1/2} \Phi_n^*(m;r) dr$$

2.3. Snapshot POD Equations

$$\lim_{\tau\to\infty}\frac{1}{\tau}\int_0^{\tau}\mathbf{u}_{\mathrm{T}}(k;m;r,t)\alpha^{(n)^*}(k;m;t)\mathrm{d}t$$

$$=\Phi_{\mathrm{T}}^{(n)}(k;m;r)\lambda^{(n)}(k;m)$$

$$\mathbf{R}\left(k;m;t,t'\right)=\int_r\mathbf{u}(k;m;r,t)\mathbf{u}^*\left(k;m;r,t'\right)r\;\mathrm{d}r$$

$$\lim_{\tau\to\infty}\frac{1}{\tau}\int_0^{\tau}\mathbf{u}_{\mathbf{T}}(k;m;r,t)\alpha^{(n)*}(k;m;t)\,\mathrm{d}t$$

$$=\Phi_{\mathbf{T}}^{(n)}(k;m;r)\lambda^{(n)}(k;m).$$

2.4. Reconstruction

The reconstruction is given by

$$q(\xi,t) - \bar{q}(\xi) \approx \sum_{j=1}^{r} a_j(t)\varphi_j(\xi) \Rightarrow$$
$$q(r,\theta,t;x) = \bar{q}(r,\theta,t;x) + \sum_{n=1}\sum_{m=0}\alpha^{(n)}(m;t)\Phi^{(n)}(r;m;x)$$

Since the snapshot pod implementation is not error-free, the reconstruction can only be recovered by writing for $\texttt{factor} \gg 0$.

$$q(r,\theta,t;x) = \bar{q}(r,\theta,t;x) + (\text{factor } \gamma)\sum_{n=1}\sum_{m=0}\alpha^{(n)}(m;t)\Phi^{(n)}(r;m;x)$$

2.5. Reconstruction

In order to reconstruct in code, caseId.fluctuation = ’off’. This is incorrect. The necessary use of (factor γ) is incorrect

3. Derivation

To derive the questioned equation, consider the integral:

$$\frac{1}{\tau}\int_0^\tau \mathbf{u}_{\mathrm{T}}(k;m;r,t)\alpha^{(n)^*}(k;m;t)dt.$$

Substitute $\mathbf{u}_{\mathrm{T}}$ with its expansion:

$$\frac{1}{\tau}\int_0^\tau \left(\sum_l \Phi_{\mathrm{T}}^{(l)}(k;m;r)\alpha^{(l)}(k;m;t)\right)\alpha^{(n)^*}(k;m;t)dt.$$

3.1. 4 Derivation

Exchange the order of summation and integration, and apply orthogonality,

$$\sum_{l} \Phi_{\mathrm{T}}^{(l)}(k;m;r)\left(\frac{1}{\tau}\int_{0}^{\tau}\alpha^{(l)}(k;m;t)\alpha^{(n)^{*}}(k;m;t)dt\right).$$

Due to the orthogonality, namely that $\alpha^{(n)}$ and $\alpha^{(p)}$ are uncorrelated

$$\langle a^{(n)}\alpha^{(p)}\rangle = \lambda^{(n)}\delta_{np}$$

all terms where $l \neq n$ will vanish, and there remains only the $l = n$ term,

$$\Phi_{\mathrm{T}}^{(n)}(k;m;r)\left(\frac{1}{\tau}\int_{0}^{\tau}\alpha^{(n)}(k;m;t)\alpha^{(n)^{*}}(k;m;t)dt\right).$$

This derivation assumes the normalization of modes and their orthogonality, along with the eigenvalue relationship to simplify the original integral into a form that reveals the spatial structure ($\Phi_{\mathrm{T}}^{(n)}$) of each mode scaled by its significance $\left(\lambda^{(n)}\right)$.

3.2. 6 Derivation

The cross-correlation tensor $\mathbf{R}$ is defined as $\mathbf{R}\left(k;m;t,t'\right) = \int_r \mathbf{u}(k;m;r,t)\mathbf{u}^*\left(k;m;r,t'\right) r \,\mathrm{d}r$. This tensor is now transformed from $[3r \times 3r']$ to a $[t \times t']$ tensor. The n POD modes are then constructed as,

$$\lim_{\tau\to\infty}\frac{1}{\tau}\int_0^{\tau}\mathbf{u}_{\mathrm{T}}(k;m;r,t)\alpha^{(n)^*}(k;m;t)\mathrm{d}t = \Phi_{\mathrm{T}}^{(n)}(k;m;r)\lambda^{(n)}(k;m).$$

4. Result Comparison Classic/Snapshot

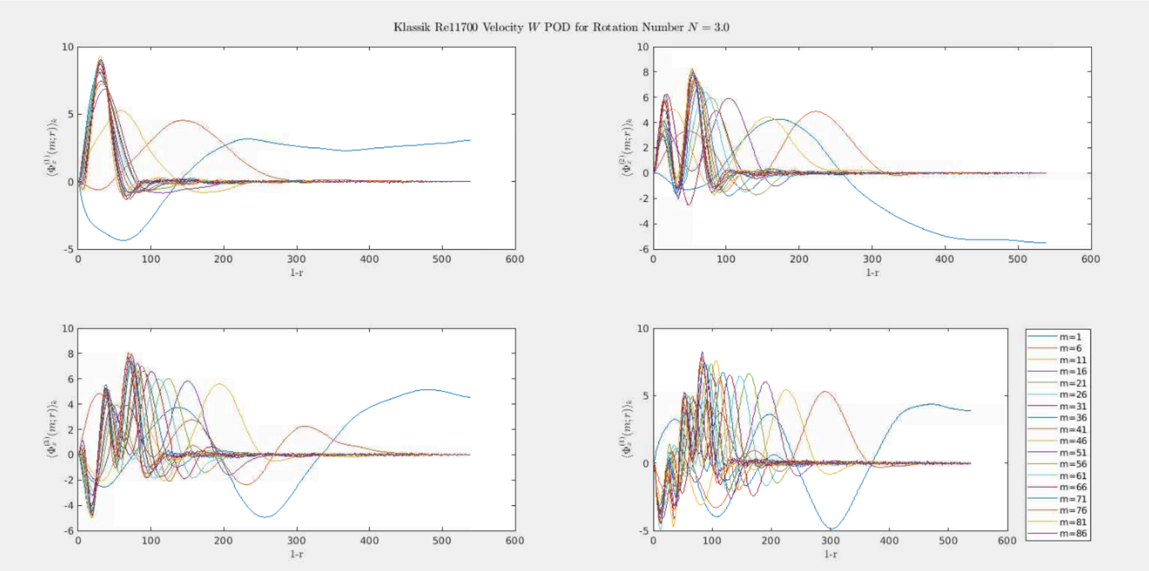
Klassik Re11700 Velocity W POD for Rotation Number $N = 3.0$
$\langle\Phi_z^{(1)}(m;r)\rangle_k$
$\langle\Phi_z^{(2)}(m;r)\rangle_k$
$\langle\Phi_z^{(3)}(m;r)\rangle_k$
$\langle\Phi_z^{(4)}(m;r)\rangle_k$
1-r
10
8
6
4
2
5
0
-2
-4
-5
-6
100
200
300
400
500
600
m=1
m=6
m=11
m=16
m=21
m=26
m=31
m=36
m=41
m=46
m=51
m=56
m=61
m=66
m=71
m=76
m=81
m=86

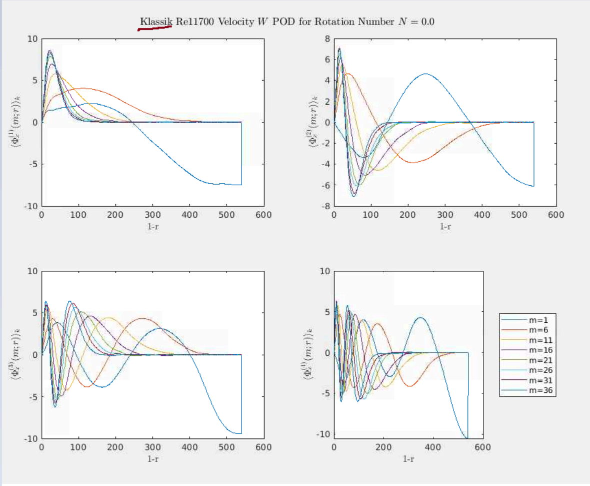
Klassik Re11700 Velocity W POD for Rotation Number $N = 0.0$
$\langle\Phi_z^{(1)}(m;r)\rangle_k$
$\langle\Phi_z^{(2)}(m;r)\rangle_k$
$\langle\Phi_z^{(3)}(m;r)\rangle_k$
$\langle\Phi_z^{(4)}(m;r)\rangle_k$
1-r
0
100
200
300
400
500
600
10
5
0
-5
-10
8
6
4
2
-2
-4
-6
-8
m=1
m=6
m=11
m=16
m=21
m=26
m=31
m=36

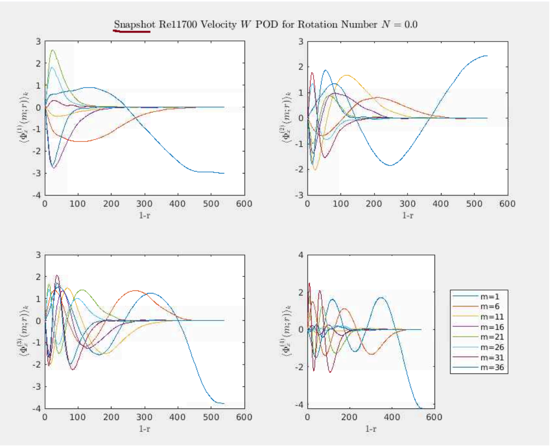
Snapshot Re11700 Velocity W POD for Rotation Number $N = 0.0$
$\langle\Phi_z^{(1)}(m;r)\rangle_k$
$\langle\Phi_z^{(2)}(m;r)\rangle_k$
$\langle\Phi_z^{(3)}(m;r)\rangle_k$
$\langle\Phi_z^{(4)}(m;r)\rangle_k$
1-r
0
100
200
300
400
500
600
4
3
2
1
0
-1
-2
-3
-4
m=1
m=6
m=11
m=16
m=21
m=26
m=31
m=36

4.3. Klassik POD S=0.0

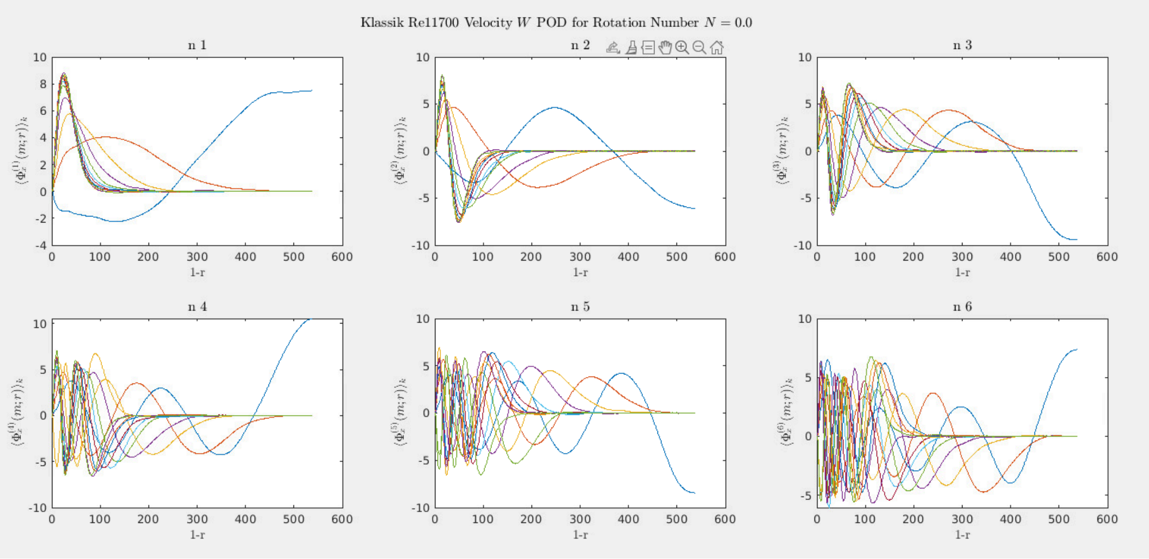

4.4. Klassik POD S=3.0

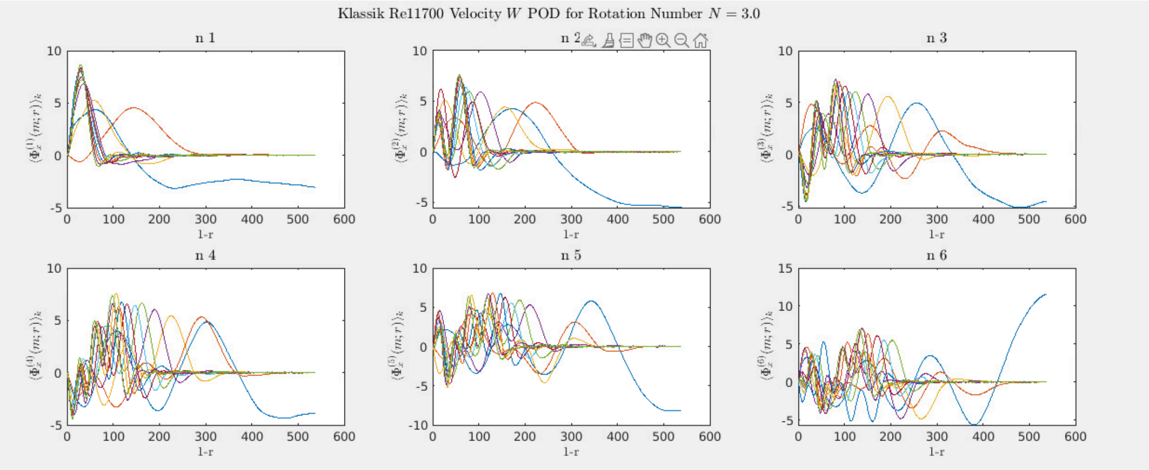

5. Energy n=0 Classic

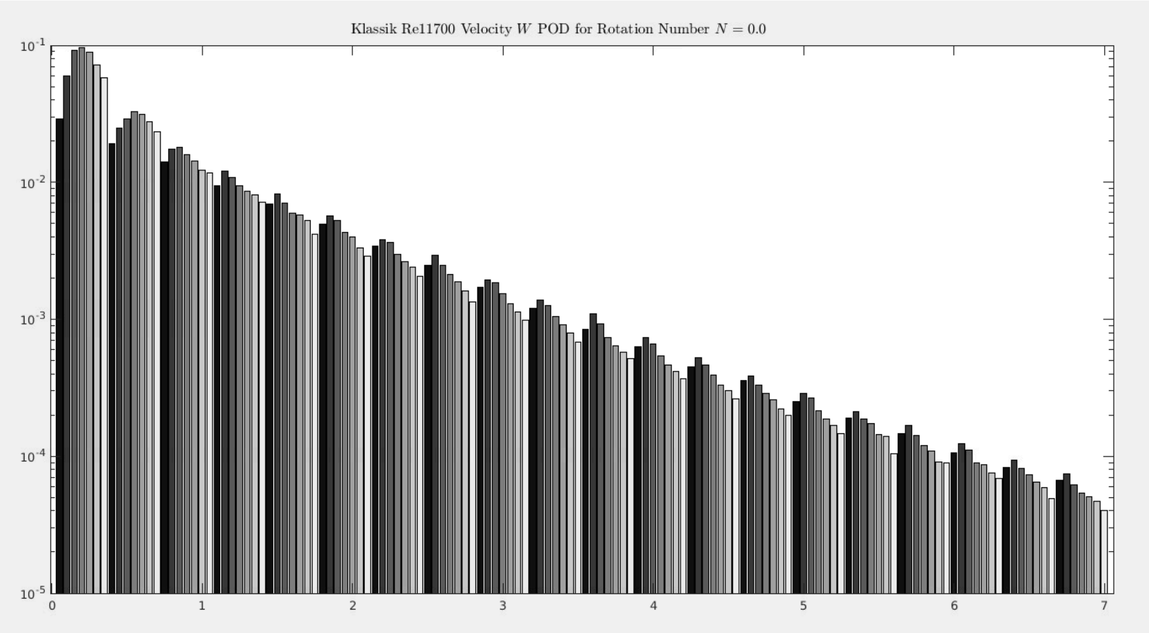

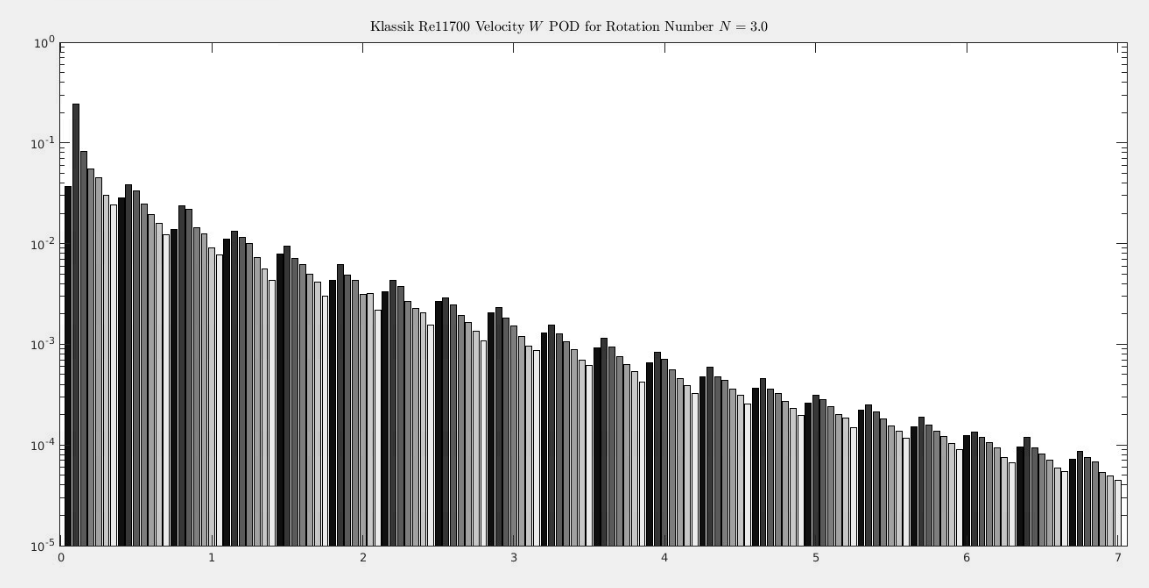
Klassik Re11700 Velocity W POD for Rotation Number $N = 3.0$
10^0
10^{-1}
10^{-2}
10^{-3}
10^{-4}
10^{-5}
0
1
2
3
4
5
6
7

6. Reconstruction

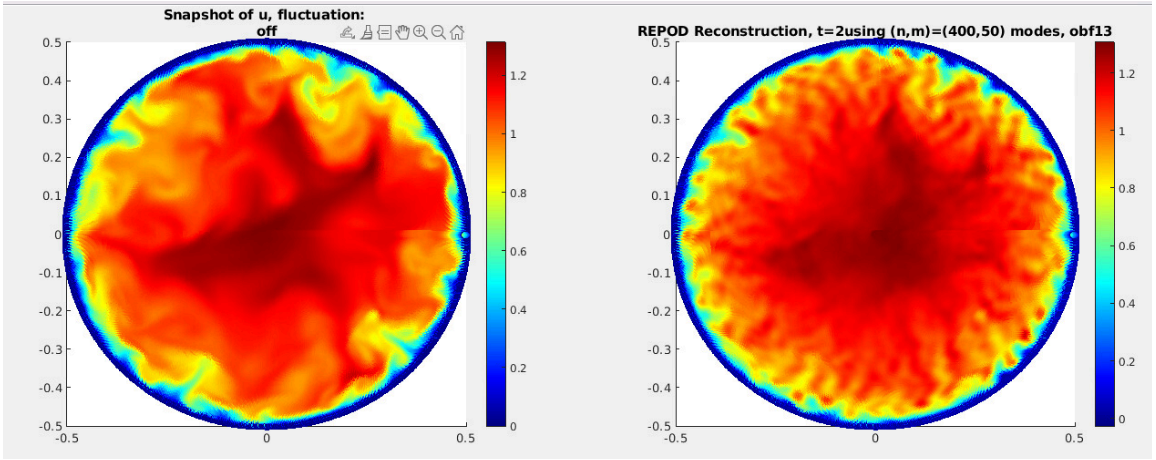

Snapshot of u, fluctuation: off

REPOD Reconstruction, t=2using (n,m)=(400,50) modes, obf13